



## 1 **Discordance Dating: A New Approach for Dating Sedimentary Alteration Events**

2

3 Jesse R Reimink<sup>1\*</sup>; Renan Beckman<sup>1</sup>; Erik Schoonover<sup>1</sup>; Max Lloyd<sup>1</sup>; Joshua Garber<sup>1</sup>; Joshua HFL  
4 Davies<sup>2</sup>; Alexander Cerminaro<sup>1,3</sup>; Morgann G Perrot<sup>2</sup>; Andrew Smye<sup>1</sup>

5

6 <sup>1</sup>Department of Geosciences, The Pennsylvania State University, University Park, PA, USA

7 <sup>2</sup>Département des sciences de la Terre et de l'atmosphère / GEOTOP, Université du Québec à  
8 Montréal, Montréal, CA

9 <sup>3</sup>Department of Geosciences, Texas Tech University, 1200 Memorial Circle, Lubbock, TX, USA

10

11 \*Corresponding Author: Jesse R. Reimink, jreimink@psu.edu

12

### 13 **Abstract:**

14 Zircon is the premier geochronometer used to date igneous and metamorphic processes, constrain  
15 sediment provenance, and monitor key events in Earth history such as the growth of continents  
16 and the evolution of the biosphere. Zircon U-Pb systematics can be perturbed by the loss or gain  
17 of uranium and/or lead, which can result in disagreement between the apparent radiometric ages  
18 of the two U-Pb decay systems – a phenomenon that is commonly termed ‘discordance’.  
19 Discordance in zircon can be difficult to reliably interpret and therefore discordant data are  
20 traditionally culled from U-Pb isotopic datasets, particularly detrital zircon datasets. Here we  
21 provide a data reduction scheme that extracts reliable age information from discordant zircon U-  
22 Pb data found in detrital zircon suites, tracing such processes as fluid flow or contact  
23 metamorphism. We provide the template for data reduction and interpretation, a suite of sensitivity  
24 tests using synthetic data, and ground-truth this method by analyzing zircons from the well-studied  
25 Alta Stock metamorphic aureole. Our results show accurate quantification of a ~23 Ma in situ  
26 zircon alteration event that affected 1.0-2.0 Ga detrital zircons in the Tintic quartzite. The  
27 ‘discordance dating’ method outlined here may be widely applicable to a variety of detrital zircon  
28 suites where pervasive fluid alteration or metamorphic recrystallization has occurred, even in the  
29 absence of concordant U-Pb data.

30

### 31 **1. Introduction:**

32 U-Pb isotopic compositions of the mineral zircon provide some of the most accurate and precise  
33 age information in the geologic record (e.g., Mattinson, 2013, 2005; Schaltegger et al., 2015;  
34 Schoene, 2014). U-Pb zircon ages from granitoids have shaped understanding of magmatic  
35 processes (e.g. Samperton et al. 2015; Barboni et al. 2015; Schaltegger and Davies 2017).  
36 Combining this geochronometer with other chemical information such as Hf-isotope  
37 compositions, oxygen isotopic compositions and trace element abundances has advanced  
38 understanding of the formation and evolution of continental crust (e.g. Belousova et al. 2010;  
39 Roberts and Spencer 2014; Reimink et al. 2023). Zircon is a refractory mineral that also resists  
40 chemical and mechanical erosion and persists in sediments over long transport distances (e.g.,  
41 Reddy et al. 2006). Detrital zircon grains in sedimentary rocks can therefore be used to track  
42 sediment provenance, basin dynamics, and the evolution of life (Andersen et al., 2019; Carter and  
43 Bristow, 2000; Fedo et al., 2003; Gehrels, 2014; Landing et al., 2021). Indeed, the oldest known  
44 fragment of Earth is in a detrital zircon grain (Froude et al., 1983).

45



46 One advantage of the U-Pb system is that it includes two independent decay chains that can be  
47 used to internally corroborate the robustness of radiometric ages.  $^{238}\text{U}$  decays to  $^{206}\text{Pb}$  while  $^{235}\text{U}$   
48 decays to  $^{207}\text{Pb}$ . A single measurement of the multi-isotopic abundances of U and Pb thus yields  
49 multiple dates. When these dates agree within analytical uncertainty, the analyses are termed  
50 ‘concordant’. ‘Discordant’ data are cases where the two U-Pb ages disagree, indicating either a  
51 mixed-age analytical domain, or that the U-Pb system has been disturbed, either through the gain  
52 or loss of U and/or Pb such that the zircon analytical volume was an open system at some point in  
53 its history.

54

55 Discordant zircon U-Pb data may be created in multiple ways, including pure Pb-loss (Nasdala et al.,  
56 1998), uranium addition (Garber et al., 2020; Grauert et al., 1974; Seydoux-Guillaume et al.,  
57 2015), a combination of both U gain and Pb loss (Andersen and Elburg, 2022), clustering of Pb  
58 into nanoparticles (Kusiak et al., 2015, 2023), mixing between two domains of different ages  
59 (Schoene, 2014 and references therein), and partial metamorphic recrystallization (e.g., Davis et  
60 al., 1968; Geisler et al., 2007; Hoskin and Black, 2002). Experimental evidence has shown that  
61 during the radioactive decay of U and Th, alpha recoil damage accumulates in the crystal lattice  
62 and can lead to interconnected pathways that may allow radiogenic Pb to escape the mineral grain  
63 and result in discordant U-Pb dates (Geisler et al., 2002, 2007; Salje et al., 1999; Trachenko et al.,  
64 2002). Many of these complex processes are difficult to disentangle at the micron scale. In  
65 particular, Pb-loss, metamorphic recrystallization, and/or diffusion-reaction processes (Geisler et  
66 al., 2007) can prove hard to differentiate from one another at the scale of a typical laser ablation  
67 analytical volume (5,000-10,000  $\mu\text{m}^3$ ).

68

69 Despite the difficulties in understanding the atomic-scale causes of U-Pb discordance in zircon,  
70 many geological processes are known to induce discordance, including the buildup of metamict  
71 domains inside zircon crystals (Nasdala et al., 1998), meteorite-impact induced shock effects  
72 (Moser et al., 2009, 2011) crystal-plastic deformation (Reddy et al., 2006), fluid induced  
73 dissolution-precipitation (Geisler et al., 2002, 2007), and metamorphic recrystallization and  
74 overgrowth that inherits some radiogenic Pb during recrystallization (Mezger and Krogstad, 1997;  
75 Schoene, 2014). It has also been suggested that highly radiation damaged zircon crystals may  
76 continually lose Pb until they experience an annealing event (Schoene, 2014).

77

78 In summary, the atomic-scale mechanics of discordance are not well understood, and most modern  
79 U-Pb studies aim to minimize its effect rather than understand or use it (see Schoene, 2014, and  
80 references therein). Thus, most studies that leverage the U-Pb system in zircon focus on concordant  
81 or upper intercept U-Pb dates (the upper intersection of a regression line through discordant data  
82 with the concordia curve) to determine the timescales of mineral formation (e.g., Vermeesch, 2021  
83 and references therein). In fact, the analytical expression of discordance has long been utilized for  
84 understanding the events that cause it. This is typically done using linear regressions (Davis, 1982;  
85 Vermeesch, 2021; York, 1968) through datasets that fall along a single chord – meaning they have  
86 one single upper intercept event (often igneous or metamorphic crystallization) and one single  
87 lower intercept event (caused by one of several potential mechanisms, discussed above). Such an  
88 approach has yielded meaningful ages for a variety of geological processes (Mezger and Krogstad,  
89 1997; Moser et al., 2009, 2011; Schoene, 2014).

90



91 Sedimentary detrital zircon analyses present a particular difficulty, and as we will show,  
92 opportunity, for dealing with discordance when compared to igneous and metamorphic zircon  
93 studies. Because each detrital zircon in a sediment may have a unique geologic history, with a  
94 correspondingly unique U-Pb disturbance and resetting history, it can be difficult to correctly  
95 interpret discordant data from detrital zircon populations. Without the constraint of a single, shared  
96 geologic history, no discordant datum can be confidently related to another datum, whether it is  
97 discordant or concordant. Therefore, in detrital zircon geochronology, the typical workflow  
98 includes discarding any analyses that do not pass a relatively strict discordance filter of 5% or 10%  
99 discordant (Gehrels, 2011). At times this can result in a significant number of data being discarded,  
100 at times up to more than 60% of the total dataset (e.g., Clemens-Knott and Gevedon, 2023). A  
101 limited number of publications have recently focused on improving methods to treat discordant  
102 detrital zircon data that would allow for the extraction of useful age information (Andersen et al.,  
103 2019; Morris et al., 2015; Olierook et al., 2021; Powerman et al., 2021; Vermeesch, 2021). These  
104 include improved filtering and treatment of discordant data (Andersen et al., 2019; Powerman et  
105 al., 2021; Vermeesch, 2021) as well as treatments that attempt to project from concordant data in  
106 either upper or lower intercepts to the opposite intercept (Morris et al., 2015; Olierook et al., 2021;  
107 Reimink et al., 2016).

108 Despite the difficulty in linking the ages between individual discordant zircon in detrital  
109 sediments, one useful assumption can safely be applied: after the deposition of the sediment, all  
110 the zircon grains have a shared thermal and geological history. In this study we leverage this  
111 assumption that post depositional U-Pb isotopic discordance may affect all zircon grains within a  
112 given sediment at the same time, in order to use discordant detrital zircon U-Pb data to investigate  
113 post-depositional geologic events (e.g. Morris et al., 2015). We also provide a robust analytical  
114 framework for determining the timing of these discordance-inducing events. We empirically show  
115 that detrital zircon grains from a sediment that was affected by contact metamorphism and fluid  
116 flow can be used to estimate the age of metamorphism and fluid alteration using zircon U-Pb  
117 discordance alone. We discuss the potential for this geochronometric tool to be applied to other  
118 types of geologic settings in sedimentary settings globally. Because discordance is commonly  
119 observed in U-Pb data, but such data are commonly rejected, we suggest that discordance is an  
120 undervalued and useful feature of detrital zircon populations, though more work is required to fully  
121 evaluate the applicability of our new analytical framework to various discordance-causing  
122 geological phenomena.

123

## 124 **2. Methods**

### 125 **2.1 Theoretical Framework**

126 Here we date in situ alteration of detrital zircons based on the approach to discordance outlined by  
127 Reimink et al. (2016). In this framework, a numerical algorithm is used to calculate the probability  
128 distribution of a zircon U-Pb dataset across a range of synthetic discordia chords that represent  
129 candidate chords spanning a defined age range. Essentially, a ‘mesh’ of potential discordia chords  
130 is created at a defined interval (e.g., every 1 Ma a new chord is created) wherein each line has a  
131 unique upper and lower intercept age (Fig. 1b). Then, the total probability that falls on each chord  
132 is calculated by determining the probability that each individual datapoint contributes to each  
133 chord, using the equations of (Davis, 1982). The total probability is summed for each chord and  
134 termed ‘likelihood’. Further details on the method can be found in Reimink et al. (2016).

135



136 Reimink et al. (2016) discussed several different  
137 normalization strategies to avoid biasing the  
138 calculated probability distributions, including  
139 homogenizing the uncertainty across a U-Pb dataset,  
140 weighting against concordance (towards discordance),  
141 and others. These normalizations can be useful to  
142 prevent artificially biasing results due to clusters of  
143 concordant data, or biasing due to heteroscedastic data  
144 (i.e., with non-uniform variance; Vermeesch, 2012). In  
145 detrital zircon datasets from rocks without post-  
146 depositional disturbances, the chord with the highest  
147 probability is likely to be associated with a group of  
148 zircon crystals that have the same upper intercept age,  
149 regardless of whether they are discordant or not. In  
150 such an analysis, the upper intercept ages the most  
151 useful output. Thus, dating a post-depositional  
152 discordance-inducing *lower-intercept* event requires a  
153 different approach. The present method modifies the  
154 original calculations to determine the most likely  
155 lower intercept age across a sample set that may have  
156 a range of upper intercept ages. For example, using  
157 the Reimink et al. (2016) calculation on a detrital  
158 sample which has a large population of near-  
159 concordant grains at 1600 Ma and experienced a Pb  
160 loss event at 30 Ma, the chord with the highest  
161 probability would likely be chord between 30 and  
162 1600 Ma (Fig. 1). However, 30 Ma lower intercept  
163 ages associated with any other upper intercept age  
164 would not be included in the probability of the 30 Ma  
165 lower intercept age, as only the 30-1600 Ma chord is  
166 considered. If a detrital zircon population contains  
167 grains that crystallized at 1000 Ma, 1200 Ma and 2700  
168 Ma and these grains also experienced *in situ* Pb-loss at  
169 30 Ma, that Pb-loss would go mostly undetected by the  
170 previous method, though each upper intercept age  
171 would be resolved independently.

172

173 To rectify this issue, here we introduce a modification  
174 to the original calculation. We add an additional step  
175 that sums the total probability aggregated to each lower intercept age. Using the example above,  
176 we add up all the probability accrued to all the lines with a lower intercept age of exactly 30 Ma.  
177 Thus, the probability accumulated by the 30-1580 Ma chord would be added to the probability  
178 accumulated by the 30-1581 Ma chord, the 30-1582 Ma chord, etc. This sum is then divided by  
179 the number of chords that have a given lower intercept age to normalize across the age range of  
180 interest. This value is then termed ‘summed likelihood’ as it is a normalized value and no longer a  
181 probability density estimate. The results of this modeling approach theoretically return an estimate

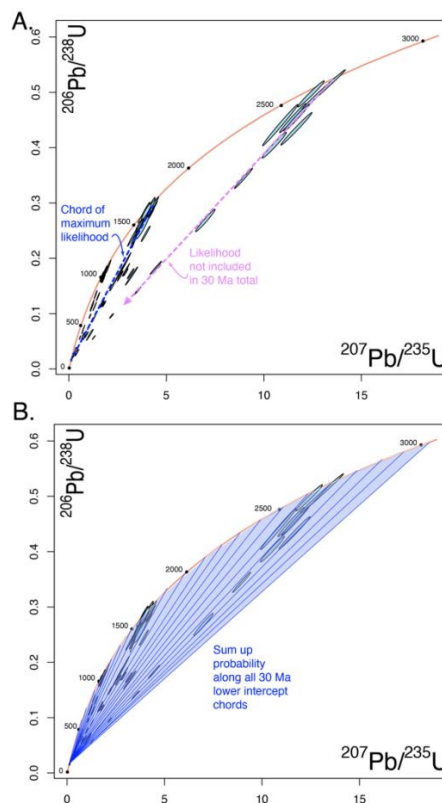


Figure 1: Example data showing why the sum probability density is required to accurately define likelihoods for lower intercept ages. In this synthetic dataset, there are many near-concordant ~1600 Ma datapoints. This cluster of near-concordant data will yield a higher probability for any chord anchored at 1600 Ma. A new method is required to evaluate the total probability contributed to any lower intercept age from a range of upper intercept ages. Panel B shows how the total probability density contributed to all lines with a 30 Ma lower intercept age could capture the likelihood of lower intercept ages in that window.



182 of the potential that a given lower intercept age may be a true post-depositional disturbance age,  
183 though it is normalized by the number of analyses and number of chords in any given model.  
184

185  
186

## 187 2.2 Calibration with Synthetic Datasets

188 To test the validity and reliability of our theoretical approach to extracting the ages of post-  
189 depositional discordance-inducing events from detrital zircons, we constructed several synthetic  
190 datasets and benchmarked our approach against traditional isochron regression techniques. To do  
191 this, we used three categories of synthetic datasets (Fig. 2):

- 192 1. A U-Pb dataset that defines a perfect discordia line with an upper intercept of 1800 Ma a  
193 lower intercept of 30 Ma
- 194 2. A dataset with three upper intercept ages (1800 Ma, 1400 Ma, 1100 Ma) all of which have  
195 discordance imposed at a shared lower intercept of 30 Ma
- 196 3. A dataset where each grain has an upper intercept age randomly selected from a range of  
197 ages (1800-1100  
198 Ma) and all have a  
199 shared lower  
200 intercept of 30 Ma.

201  
202 For each of the three  
203 categories, a synthetic data  
204 population was generated  
205 that contained 150 U-Pb data  
206 points. Each data point was  
207 randomly assigned an upper  
208 intercept and lower intercept  
209 age based on the model  
210 structure. In the case of the  
211 perfect line, all data points  
212 had the same upper intercept  
213 age. Then, each data point  
214 was assigned a random  
215 amount of discordance  
216 between 99.95% and 1%,  
217 selected from a flat  
218 probability distribution. This  
219 random discordance accounts  
220 for the fact that each  
221 individual zircon grain,  
222 and indeed portions of grains,  
223 have differing resetting  
224 susceptibilities due to a  
225 variety of factors. The ratios  
226 of interest for each data point were assigned a random uncertainty value between 2-5% of their  
227 isotopic composition.

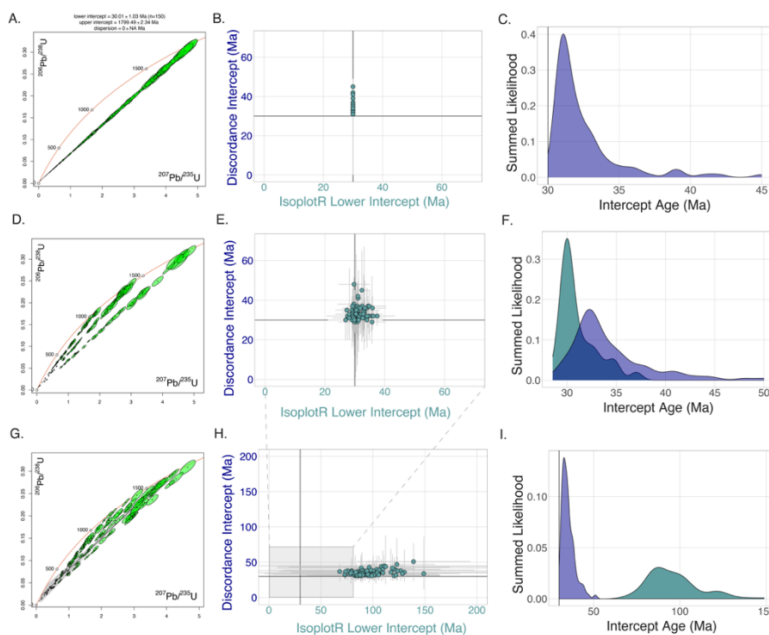


Figure 2: Input data and results from a synthetic data modeling procedure. Panels A, D, and G show examples of the synthetic input data, plotted on U-Pb concordia diagrams. The center panels (B, E, H) show the mean and uncertainties of the Isoplot R regression lower intercept age compared to the lower intercept values derived from the discordance modeling approach. Each data point represents a single synthetically generated dataset of 150 data points. The rightmost pane (C, F, I) shows the distribution of lower intercept ages from each method with the blue curve representing the ages produced by the discordance model and the green curve representing the ages generated by the model 1 regression in IsoplotR. Note the change of scale in Panel H compared to E and B.



228

229 Each synthetic data set of 150 points was then evaluated in two ways. First, the traditional U-Pb  
230 regression ages were derived using the commonly used “York fit” approach (York, 1968) as  
231 implemented in IsoplotR (Vermeesch, 2018), from which the upper and lower intercept ages were  
232 extracted. For the model constructed with three discrete upper intercept ages, we calculated three  
233 independent isochron regressions in IsoplotR, one for each population of synthetic data with a  
234 unique upper intercept age, and then calculated the weighted mean lower intercept age of these  
235 three regressions. Second, the data were input into our discordance modeling procedure and the  
236 maximum sum likelihood was extracted as well as the full width, half max of that peak – a measure  
237 of the spread in our modelled spectral data.

238

239 This entire procedure was repeated 100 times for each of the three categories, resulting in 300  
240 model runs. The results from the outputs of the ‘York fit’ approach (model 1 regression in Isoplot  
241 R) are compared to our discordance modeling approach. Figure 2 shows the three different types  
242 of models, with the calculated lower and upper intercept ages from each individual dataset. Each  
243 category of example dataset is

244 synthesized 100 times, and  
245 derivative calculations are shown  
246 for each type of dataset. Note that  
247 in Fig. 2C, the IsoplotR lower  
248 intercepts are tightly bound at 30  
249 Ma so the probability density is not  
250 shown here. Figure 3 shows the  
251 discordance dating outputs in more  
252 detail, with individual age  
253 distributions shown from the  
254 discordance dating outputs. It is  
255 important to note that our  
256 discordance dating approach  
257 makes no assumptions about the  
258 distribution of the underlying data  
259 and does not require linearity between the  
260 data points to perform linear  
261 regression calculations. As such,  
262 the discordance dating approach is  
263 more agnostic with regard to the  
264 distribution of the underlying data,  
265 and therefore yields more accurate  
266 results for complex datasets (Fig.  
267 4). The discordance dating  
268 approach can also yield  
269 asymmetric likelihood  
270 distributions (Fig. 3 center panels) due to the structure of the underlying U-Pb data set.

271

272 The outputs of each calculation method are summarized in Fig. 4. For the simplest scenario, the  
273 perfect discordia line, the IsoplotR York-fitting calculations correctly determine the lower intercept

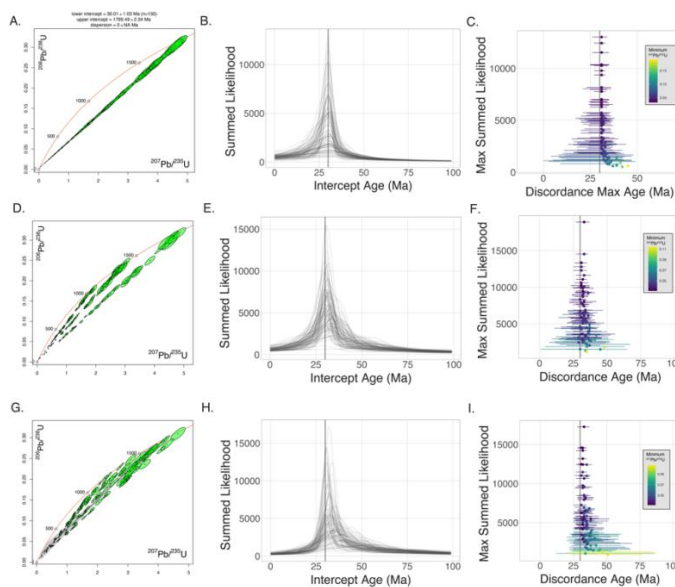


Figure 3: Results from the three sets of model runs for the discordance modeling procedure. The left panels show examples of the input datasets (same as Fig. 2). The central panels show lower intercept likelihood curves for the 100 model runs in each category of model. The right panels show the peak location, the uncertainties (derived by a full-width half-max calculation), and are colored according to the lower  $^{207}\text{Pb}/^{235}\text{U}$  value in a given synthetic dataset. The discordance modeling procedure yields similar results independent of the input data type.



274 age of 30 Ma with excellent precision (mean = +/- 0.33 Ma), while the discordance dating model  
275 has larger uncertainties associated with the lower intercept age. As shown in Figure 3, the FWHM  
276 of peaks returned by the discordance dating procedure are positively correlated to the peak height,  
277 where higher peaks return smaller FWHM uncertainty estimates. Sharp peaks are, in turn,  
278 correlated to how close the ‘youngest’  
279 analysis is to the 30 Ma lower intercept,  
280 where precise lower intercept estimates are  
281 typically derived from populations of data  
282 points that have some analyses close to the  
283 concordia curve near the lower intercept  
284 age. It is expected – and observed (Fig. 4)  
285 – that the York fitting procedure used in  
286 IsoplotR should outperform the  
287 discordance dating algorithm with respect  
288 to precision on the lower intercept for the  
289 simplest case where data can be regressed  
290 on a single line. However, both methods  
291 still recover the accurate lower intercept  
292 age within uncertainty.

293  
294 When considering more complex U-Pb  
295 populations (for example the lower panels  
296 in Fig. 4) that contain many primary  
297 (upper intercept) U-Pb ages, the  
298 discordance dating procedure outperforms  
299 single linear regression and weighted  
300 means of multiple linear regressions, as  
301 used in Isoplot calculations. In the case of  
302 having multiple discrete upper intercept  
303 ages (middle panel in Fig. 4), the discordance dating, although less precise, provides improved  
304 accuracy and likely a more reliable uncertainty estimate. For the case of many upper intercept ages  
305 (lowest panel in Fig. 4) discordance dating is both more accurate (fewer model runs predict lower  
306 intercept ages that are outside uncertainty of the ‘true’ age of 30 Ma – 1/100 for discordance dating,  
307 88/100 for IsoplotR) and more precise than the single line regression.

308  
309 This is also an expected result. A linear regression method is poorly suited for highly scattered data  
310 that do not share a common linear relationship, highlighting the difficulty in extracting valuable  
311 U-Pb resetting age information from discordant data. In comparison, the discordance dating  
312 method is robust regardless of the nature of the distribution of original U-Pb crystallization ages  
313 that experience a shared discordance-inducing event. We interpret this result to support the use of  
314 the method for a new approach to evaluate of the distribution of discordant data in U-Pb space.

315  
316 This exercise also sets expectations for the uncertainties and potential biases on the lower intercept  
317 that can be derived from this procedure. Focusing on the models with a range of upper intercept  
318 ages, discordance dating returns an uncertainty envelope that is on average ~20 Ma (average peak  
319 width using FWHM on each peak). However, the central peak of the discordance dating (the

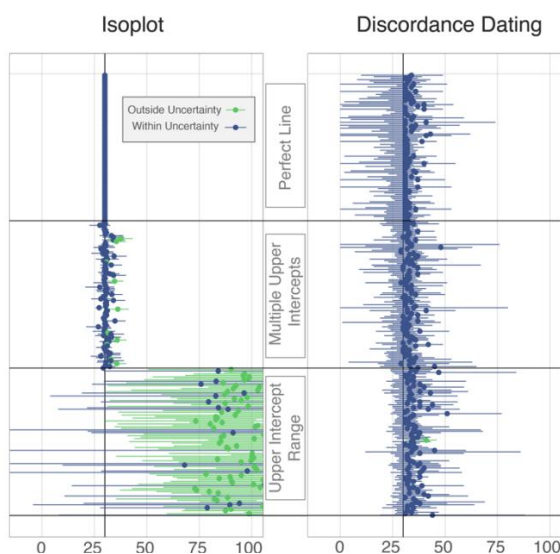


Figure 4: A comparison of the lower intercept ages and uncertainties for the Isoplot regression calculations and the Discordance Dating method for all synthetic data runs. Each point is a unique dataset and the uncertainties are given for each regression point. The color of each point corresponds to whether the lower intercept age is within uncertainty of the pre-defined lower intercept of 30 Ma or not. The Discordance dating method provides more reliable results across a range of data types than simple linear regression models. d



320 maximum likelihood lower intercept age) for these 100 models is 35 Ma +/- 3.4 Ma (1SD). The  
321 discordance dating procedure infrequently returns peak centers that are younger than 30 Ma,  
322 though it commonly returns peak centers older than 30 Ma. This bias to older lower intercept ages  
323 is likely due to the sensitivity of the discordance dating procedure to the position of the youngest  
324 point in any dataset – or the most ‘reset’ grain in any population. This is also important for our  
325 later interpretations – discordance dating is highly unlikely to return a max peak position that is  
326 too young (assuming no modern-aged discordance in the population), and any maximum peak  
327 position can likely be interpreted as a maximum age value for the true lower intercept resetting  
328 age.

329

### 330 **3. Alta Stock Detrital Zircon Results**

#### 331 **3.1 Methods and Results**

332 To test and validate the discordance dating strategy outlined above, we conducted a laser ablation  
333 ICPMS analytical campaign targeting a well-studied metamorphic aureole with a known fluid-  
334 alteration history. We sampled a metasedimentary unit from the well-studied Alta stock  
335 metamorphic aureole, Utah (Brenner et al., 2021; Cook et al., 1997; Moore and Kerrick, 1976;  
336 Stearns et al., 2020). The Alta stock intruded a suite of mid-Paleozoic sedimentary rocks in the late  
337 Paleogene (36-30 Ma; Stearns et al., 2020 and references therein) and was exposed through  
338 Miocene-aged uplift and tilting along the Wasatch fault and Pleistocene glaciations and erosion in  
339 Little Cottonwood Canyon (Stearns et al., 2020 and references therein). The Alta stock is one of a  
340 handful of plutons in the region that formed between ~36 Ma and ~30 Ma (Bromfield et al., 1977;  
341 Crittenden et al., 1973; Kowallis et al., 1990; Stearns et al., 2020). Titanite and zircon age  
342 constraints from the Alta stock indicate it was emplaced near the early stages of this interval  
343 (Crittenden et al., 1973; Stearns et al., 2020). Stock emplacement was accompanied by contact  
344 metamorphism in the host units and hydrothermal fluid alteration (Brenner et al., 2021; Cook et  
345 al., 1997; Moore and Kerrick, 1976). This fluid flow was primarily down-temperature and was  
346 focused in mixed carbonate-siliciclastic beds facilitated by porosity-forming decarbonation  
347 reactions (Cook et al., 1997). Previous geochronology on magmatic and overprinted zircon along  
348 with magmatic and metamorphic aureole titanite phases indicates Alta stock contact  
349 metamorphism extended from >30 to 25 Ma (Stearns et al., 2020). This, in combination with trace-  
350 element thermobarometry led Stearns et al. (2020) to conclude that the earliest (36-30 Ma) phases  
351 were dominated by high temperature plutonism and metamorphism, whereas hydrothermal  
352 alteration activity remained active until ~23 Ma, particularly at the margins of the Alta stock.

353

354 We focused on a single sample of the Cambrian Tintic quartzite. This was collected ~200m from  
355 the contact with the Alta stock contact, above the tremolite-in isograd, and experienced  
356 metamorphic and fluid-alteration temperatures of ~450°C (Brenner et al., 2021; Cook et al., 1997).



357 This metamorphic and alteration history,  
358 combined with the ages of detrital zircons  
359 found in the Tintic formation ranging from  
360 1.0 Ga to <2.5 Ga (Matthews et al., 2017),  
361 provides an ideal testing ground for  
362 determining the accuracy and precision of  
363 the discordance dating technique.

364

365 Detrital zircons were isolated using  
366 standard crushing and mineral separation  
367 practices. Limited hand picking of zircons  
368 was conducted in an attempt to avoid  
369 biasing the results at that stage. Zircons  
370 were selected from other heavy minerals,  
371 but no preference was given for quality or  
372 morphology of zircon grains at this picking  
373 stage. Zircons were mounted in epoxy,  
374 polished to midsection, imaged using  
375 secondary electron imaging techniques,  
376 and subsequently analyzed by laser  
377 ablation techniques following the methods  
378 of (Cipar et al., 2020; Schoonover et al.,  
379 2024). A Teledyne/Photon Machines  
380 Analyte G2 excimer laser was used, with a  
381 Helex2 ablation cell, for all laser ablation  
382 work.

383

384 Zircon U-Pb and trace element data was  
385 collected in three sessions from Feb. 2023  
386 to May 2023. Two sessions, on Feb. 28<sup>th</sup>,  
387 2023 and March 3<sup>rd</sup>, 2023, collected U-Pb-  
388 TE on the Thermo Scientific iCapRQ  
389 quadrupole mass spectrometer in the  
390 LionChron analytical facility. Isotopes  
391 measured included  $^{27}\text{Al}$ ,  $^{29}\text{Si}$ ,  $^{44}\text{Ca}$ ,  $^{51}\text{V}$ ,  $^{57}\text{Fe}$ ,  $^{146}\text{Nd}$ ,  $^{147}\text{Sm}$ ,  $^{163}\text{Dy}$ ,  $^{172}\text{Yb}$ ,  $^{204}\text{Pb}$ ,  $^{206}\text{Pb}$ ,  $^{207}\text{Pb}$ ,  $^{232}\text{Th}$ ,  
392 and  $^{238}\text{U}$ . The analytical session on May 30<sup>th</sup>, 2023 utilized split stream techniques, where  $^{204}\text{Pb}$ ,  
393  $^{206}\text{Pb}$ ,  $^{207}\text{Pb}$ ,  $^{232}\text{Th}$ ,  $^{235}\text{U}$  and  $^{238}\text{U}$  were analyzed on the Thermo Scientific Element XR ICPMS  
394 system and  $^7\text{Li}$ ,  $^{23}\text{Na}$ ,  $^{27}\text{Al}$ ,  $^{29}\text{Si}$ ,  $^{31}\text{P}$ ,  $^{43}\text{Ca}$ ,  $^{45}\text{Sc}$ ,  $^{49}\text{Ti}$ ,  $^{55}\text{Mn}$ ,  $^{57}\text{Fe}$ ,  $^{59}\text{Co}$ ,  $^{60}\text{Ni}$ ,  $^{85}\text{Rb}$ ,  $^{88}\text{Sr}$ ,  $^{89}\text{Y}$ ,  $^{90}\text{Zr}$ ,  
395  $^{93}\text{Nb}$ ,  $^{119}\text{Sn}$ ,  $^{133}\text{Cs}$ ,  $^{137}\text{Ba}$ ,  $^{139}\text{La}$ ,  $^{140}\text{Ce}$ ,  $^{141}\text{Pr}$ ,  $^{146}\text{Nd}$ ,  $^{147}\text{Sm}$ ,  $^{153}\text{Eu}$ ,  $^{157}\text{Gd}$ ,  $^{159}\text{Tb}$ ,  $^{163}\text{Dy}$ ,  $^{165}\text{Ho}$ ,  $^{166}\text{Er}$ ,  
396  $^{169}\text{Tm}$ ,  $^{172}\text{Yb}$ ,  $^{175}\text{Lu}$ ,  $^{180}\text{Hf}$ , and  $^{182}\text{W}$  were measured on the iCapRQ quadrupole mass spectrometer.  
397  $^{235}\text{U}$  was calculated from  $^{238}\text{U}$  and the U-isotopic composition of 137.818 (Hiess et al., 2012) due to  
398 low  $^{235}\text{U}$  signals. NIST 612 glass was used as a trace-element primary reference material and zircon 91500 was used as a primary reference material for U-Pb isotopic measurements. Uranium-  
399 lead and trace element data was filtered, standardized, and normalized using the Iolite data  
400 reduction software.

401  
402

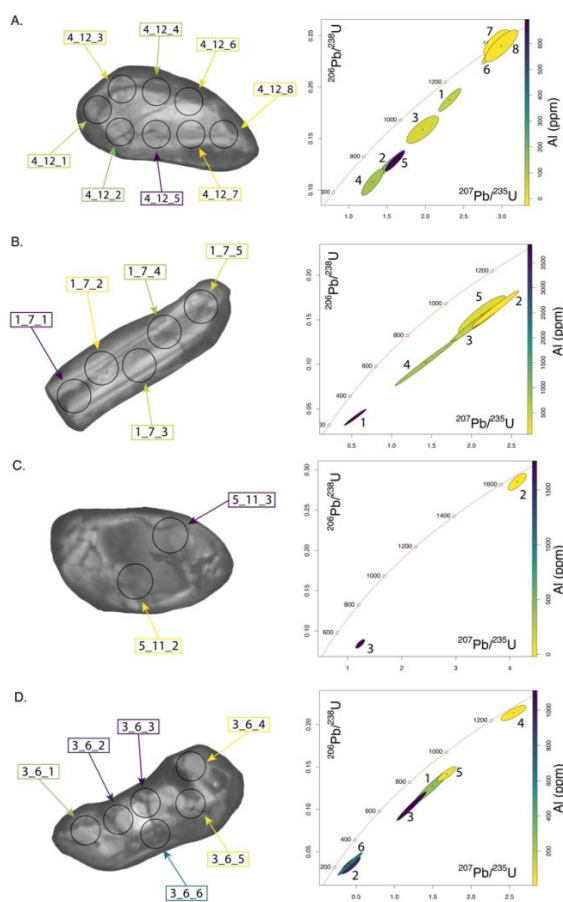


Figure 5: Representative Tintic detrital zircons and their U-Pb isotopic data. Each analysis point is labeled, where color labels correspond to the Al concentration of the analytical volume. The color scales vary between grains. Spot sizes are 30  $\mu\text{m}$  in diameter.



403 Secondary zircon reference materials include Piexe, GJ-1, Plesovice, and MudTank. Secondary  
404 reference material U-Pb results are shown in the supplements. The only session where a secondary  
405 reference material's U-Pb age was > 2% outside of the accepted age was in the March 3<sup>rd</sup> session,  
406 where GJ-1 had an average  $^{206}\text{Pb}/^{238}\text{U}$  age ~3% lower than the accepted age. However, during the  
407 same session Piexe returned a  $^{206}\text{Pb}/^{238}\text{U}$  age in line with the accepted age. Position-dependent  
408 fractionation may have played a role in the slightly increased inaccuracy of the GJ-1 zircon during  
409 this analytical session. All other sessions returned secondary reference material results within 2%  
410 of the accepted ages (see supplementary materials for data and results).

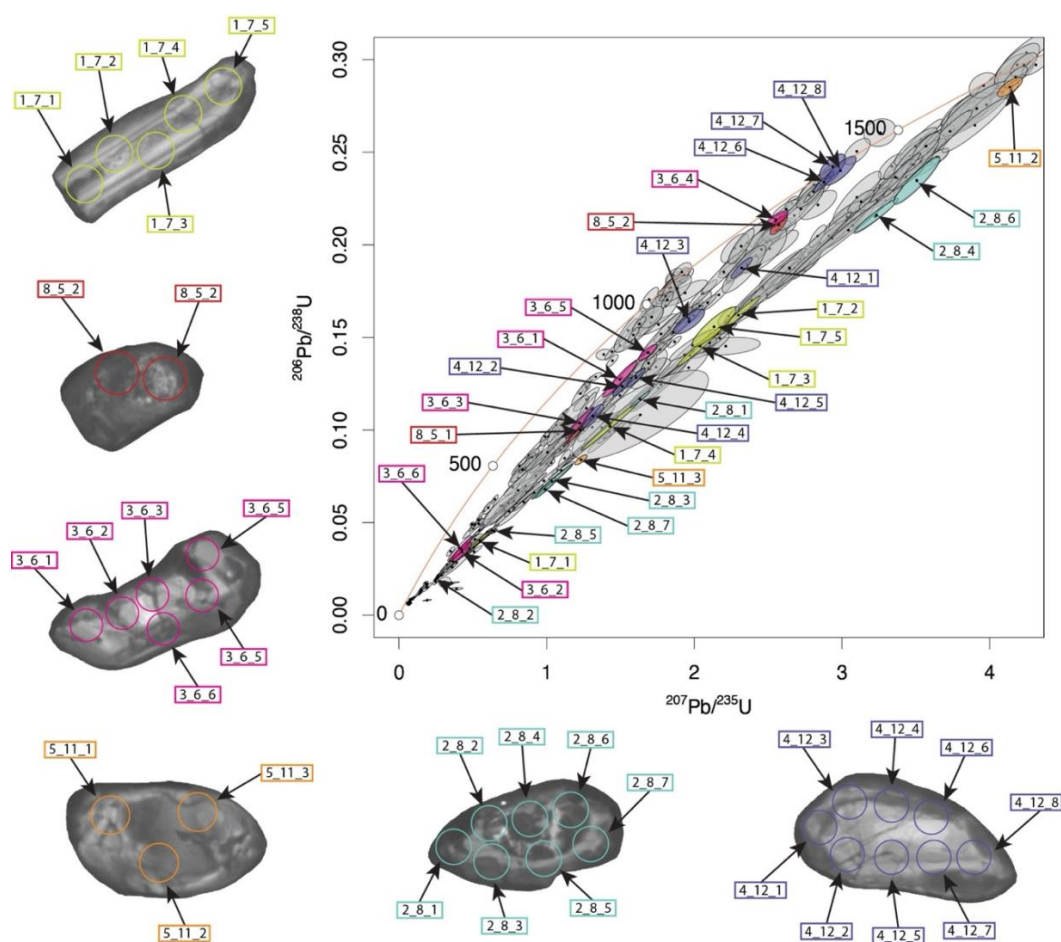


Figure 6: U-Pb data from detrital zircons extracted from the Tintic quartzite sample studied in this work. Zircon secondary electron microscope images are shown with spot locations correlated to individual data points. For scale, laser spots are all 30  $\mu\text{m}$ .

411  
412 Detrital zircons from the Tintic formation show a wide range of igneous and metamorphic/fluid  
413 alteration textures. Many (Fig. 5a,b) contain internal zones with apparent oscillatory zoning while  
414 others (Fig. 5a,c,d) show clear metamorphic rims along with wispy internal disturbance textures



415 (Corfu, 2003). While the full dataset contains a wide range of U-Pb isotopic discordance (Fig. 6),  
416 individual grains can often display a wide range of internal age and chemical variability (Figs.  
417 5,6).

418

419 Zircons from this sample show a range of  $^{207}\text{Pb}/^{206}\text{Pb}$  ages between 1 Ga and 1.8 Ga, and a wide  
420 range in  $^{206}\text{Pb}/^{238}\text{U}$  ages (Figs. 5,6), leading to a large spread in the associated discordance. In  
421 typical detrital zircon work, where filtering for concordance is normal (Gehrels, 2014), the vast  
422 majority of these analyses would be filtered out and not considered further. The U-Pb data were  
423 used as inputs into the updated version of the discordance modeling algorithm of Reimink et al.  
424 (2016). The results of modeling are shown in Fig. 7. As discussed previously, the discordance  
425 modeling produces a ‘sum likelihood’ value across a range of lower intercept ages, in this case  
426 from 0 to 50 Ma. Note that the lower intercept range is independent of the model outputs as the  
427 data reduction is conducted geometrically. The most likely lower intercept age is definitively  
428 greater than 0 Ma, as the model is capable of modeling future ages and likelihood declines rapidly  
429 prior to 0 Ma. The peak in likelihood is ~23 Ma, and sensitivity tests (Section 3.2) show that the  
430 best fit age is 22-25 Ma.



431

### 432 3.2 Sensitivity Analysis

433 In order to test the sensitivity of the results shown in Fig. 7 to individual data points or groups of data points and conduct uncertainty analysis, we conducted a bootstrapped resampled modeling routine. The full Tintic Formation dataset was resampled with a pick-and-replace method to create 1000 synthetic datasets that contained the same number of data points as the original dataset (407 analyses). Each of these synthetic datasets was put through the discordance dating method and summed likelihood lower intercept ages were calculated. The maximum summed likelihood values and the ages of those maximum values were aggregated for each synthetic dataset. Figure 6B shows the distribution of the 1000 resampled discordance models, the majority of which have lower intercept peaks that cluster between 18-28 Ma. These ages are centered on the youngest ages documented by Stearns et al. (2020) from endoskarn titanites with ages down to 23 Ma which have been found in the Alta Stock metamorphic halo. Our data show that discordance induced by metamorphic resetting and/or fluid induced Pb-loss at this time affected a large portion of detrital zircons in the Tintic formation and validates our theoretical approach to discordance dating of disturbances in detrital zircons.

461

462 Non-radiogenic Pb, termed ‘common lead’, can be found in meaningful concentrations in zircon, particularly metamorphic or otherwise perturbed zircon crystal lattices (Andersen, 2002; Schoene, 2014). The correction of this common Pb is necessary for accurate and precise geochronology, and several algorithms can be applied to remove the effect of common Pb from the U-Pb age calculations. The Tintic formation detrital zircon analyses do contain some common Pb, with higher concentrations present in a fraction of the more discordant analyses. To test if common Pb corrections influence our discordance dating methodology, we analyzed the Tintic formation zircons after two different common Pb correction types, in addition to the uncorrected data shown in Fig. 7 (green line in A). These results are shown in Figure 8. First, we apply various common Pb correction methods to subtract the contribution of ‘common Pb’ to the  $^{206}\text{Pb}$  and  $^{207}\text{Pb}$  signals. One common method (e.g., Schoene, 2014) is to use

471 analyses do contain some common Pb, with higher concentrations present in a fraction of the more discordant analyses. To test if common Pb corrections influence our discordance dating methodology, we analyzed the Tintic formation zircons after two different common Pb correction types, in addition to the uncorrected data shown in Fig. 7 (green line in A). These results are shown in Figure 8. First, we apply various common Pb correction methods to subtract the contribution of ‘common Pb’ to the  $^{206}\text{Pb}$  and  $^{207}\text{Pb}$  signals. One common method (e.g., Schoene, 2014) is to use

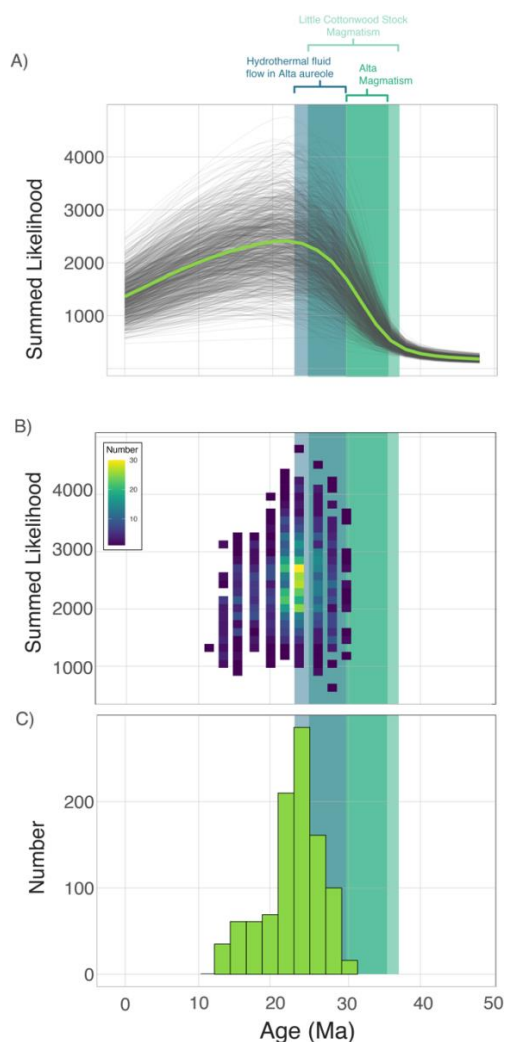


Figure 7: Outputs from discordance dating of Tintic formation zircons, and bootstrapped resampling efforts. A shows the summed likelihood lower intercept results of discordance dating. B shows the age and maximum sum likelihood value for each maximum value calculated from the curves shown in A. C shows a histogram of the peak positions in Ma.



477 the  $^{204}\text{Pb}$  signal as an indication of the amount of common Pb, assume a Pb isotope composition  
478 using the Stacey-Kramers (Stacey and Kramers, 1975) global Pb-isotope evolution model, and  
479 subtract this common  $^{206,207}\text{Pb}$  from the presumably radiogenic portion of the Pb. Another method  
480 involves the iterative solution to a series of equations assuming that the U/Th has not been  
481 disturbed and any time of Pb-loss is known (Andersen, 2002) – the latter assumption makes the  
482 method inappropriate for use with highly discordant data where the age of isotopic disturbance is  
483 unknown, data similar to the Tintic data evaluated here. Nevertheless, we show that there is little  
484 difference between the outputs of our discordance dating model on U-Pb data corrected using  
485 different common Pb calculations (Fig. 8), suggesting that the discordance dating lower intercept  
486 age is robust from the influence of common Pb, at least for the Tintic Formation zircon dataset  
487 evaluated here.

488

### 489 3.3 Causes of Discordance

490 The theoretical underpinnings of the  
491 discordance dating approach outlined here  
492 do not require any specific process to  
493 generate discordance in detrital zircon U-Pb  
494 data. As discussed previously, reliably  
495 isolating a discordance-inducing process  
496 requires additional in situ measurements  
497 (e.g., Raman mapping, e.g., Nasdala et al.,  
498 1998) that is outside the scope of the present  
499 manuscript.

500

501 However, here we discuss our dataset in  
502 light of the current understanding of  
503 discordance and outline possible avenues  
504 forward. Of the range of viable discordance  
505 mechanisms outlined above, we focus on  
506 two categories: 1) dynamic metamorphic  
507 recrystallization or overgrowth (Hoskin,  
508 2003; Hoskin and Black, 2002; Schoene,  
509 2014) and 2) fluid-mediated without  
510 significant recrystallization (Geisler et al.,

511

512 2002; Nasdala et al., 2010). These two categories of processes likely have many shared  
513 characteristics, such as the ‘dissolution-recrystallization’ process whereby hydrous fluids  
514 preferentially infiltrate decay-damaged portions of the zircon lattice and initiate structural  
515 annealing (Geisler et al., 2007). Such altered and annealed domains can contain micro-inclusions  
516 of other mineral phases such as thorite, xenotime, and uraninites, among others.

517

518 To distinguish between fluid-mediated Pb-leaching vs. recrystallization of zircon domains, we  
519 examined trace element data collected on the same zircon analyses spots via LASS measurements.  
520 If discordance in the Tintic zircon population was caused by metamorphic overprinting or  
521 recrystallization, the most discordant zircon analyses would be expected to have low Th/U typical  
522 of metamorphic zircon growth zones (Hoskin, 2003).

522

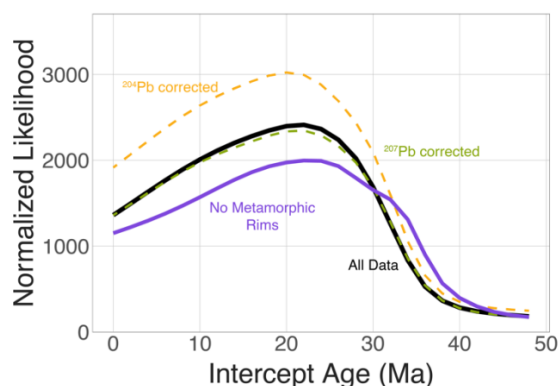


Figure 8: Plot showing the summed lower likelihood for Sample 2 U-Pb data with various common-Pb corrections applied. The black curves shows the base data with no common Pb correction. The orange curve shows the same data with a  $^{204}\text{Pb}$  and Stacey-Kramers common Pb correction applied. The green curve shows the  $^{207}\text{Pb}$  or Anderson correction applied to the same data. The purple line shows the lower intercept result for data that excludes all analyses that included a metamorphic rim growth feature. There is little change in the peak position across these various datasets, indicating that common Pb is unlikely to be affecting our results.



523 The Tintic zircons analyzed here show distinct trends  
524 between higher U concentrations and increased  
525 discordance, and correspondingly lower Th/U (Fig. 9).  
526 More discordant analyses also have higher Th, higher Al,  
527 and among the most discordant analyses occasionally  
528 higher  $^{204}\text{Pb}$  (Figs. 5,9). The steady increase in U and Th  
529 concentrations with increasing discordance could be  
530 generated in two distinct ways. First, metamorphic zircon  
531 can contain higher U and Th concentrations than typical  
532 igneous zircons (e.g., Garber et al., 2020). So, increasing  
533 U+Th concentrations could be an indication of increasing  
534 metamorphic zircon growth in particular analytical  
535 volumes. This hypothesis is corroborated by an average  
536 decrease in Th/U with increasing discordance, typically  
537 used as a monitor for metamorphic zircon growth  
538 (Hoskin, 2003). This might suggest that discordant Tintic  
539 zircon domains were sites of preferential nucleation for  
540 metamorphic overgrowths.

541  
542 An alternative hypothesis based on fluid ingress into  
543 damaged zircon is, at this stage, equally viable. In this  
544 model, high U+Th igneous zircon domains led to more  
545 radiation damage from zircon crystallization until the ~30  
546 Ma fluid alteration event. Indeed, discordance is highly  
547 correlated with the alpha dose of analytical volumes in the  
548 Tintic formation zircon population. At 30-25 Ma, reactive  
549 fluids may have preferentially infiltrated radiation-  
550 damaged (old, high U+Th) zircon regions, removed  
551 radiogenic Pb, introduced non-stoichiometric elements  
552 such as Al, and therefore induced discordance.

553  
554 At the current time, definitively distinguishing between  
555 these two types of isotopic disturbance and resetting  
556 processes is not possible. However, differentiation could  
557 be done by, for instance, combining zircon U-Pb-TE  
558 data with Raman spectrometer analyses of altered  
559 domains that could quantify the crystallinity of the  
560 zircon lattice (Anderson et al., 2020; Nasdala et al.,  
561 2010; Resentini et al., 2020; Zhang et al., 2000) and help  
562 determine which of these two models, metamorphic  
563 recrystallization and/or fluid-induced Pb loss, was a  
564 dominant Pb-loss-inducing process in the Tintic zircon population. However, this would need to  
565 be accomplished prior to destructive analyses for U-Pb-TE via laser ablation.

566  
567 An important consideration is what types of conditions are required to create the high degree of  
568 discordance that we have shown to be useful for geochronological studies. Though definitive

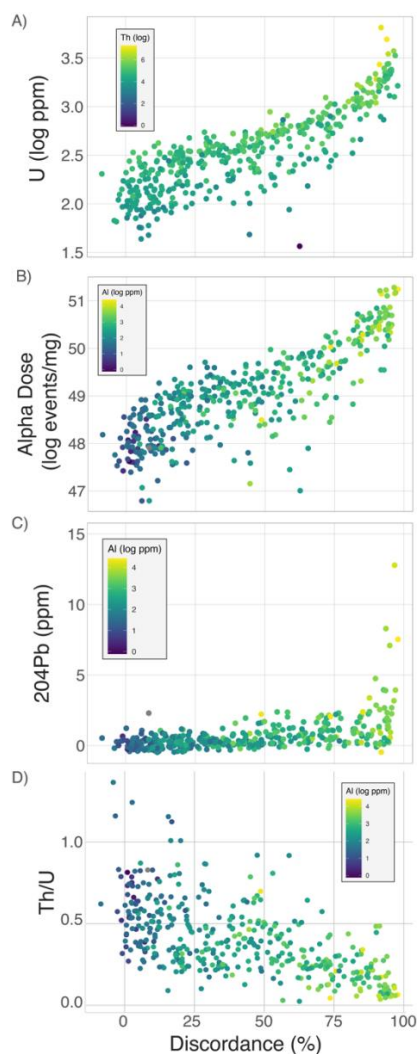


Figure 9: Zircon trace element data plotted as a function of discordance in the U-Pb system. Note that  $^{204}\text{Pb}$  is frequently at negligible concentrations such that background corrections generate apparent negative values. Note that one data point with artificially negative  $^{204}\text{Pb}$  concentrations is removed from the plot.



569 answers to this question will require more analyses from other locations with different styles of  
570 discordance, we can speculate using the Tintic dataset generated here. Zircon analyses from the  
571 Tintic formation in the Alta metamorphic aureole were qualitatively categorized by their visible  
572 morphology during SEM imaging in the following way: 1) the percentage of the spot location that  
573 included obvious metamorphic rim growth was determined and given a value of 0%, 25%, 50%,  
574 75%, or 100%; 2) similarly, the percentage of the analytical spot location that included mottled  
575 and recrystallized zones was determined, and assigned the same discrete percentage classifications  
576 as the metamorphic rims; 3) a qualitative estimate of the amount of ‘fractures’ included in the  
577 analytical area was determined and the spots were assigned a value of 0 – no fractures, to 3 – many  
578 fractures. Examples of the zircons analyzed are shown in Figures 5 and 6, and the grain numbers  
579 with each category are given in Table 1. Note 34 analyses do not have classification systems as the  
580 SEM images were not of sufficient quality to determine the morphology.

581

582 *Table 1: Classification table of analytical spot morphologies. Each spot is categorized according to three categories according to*  
583 *the CL imaging of spot locations. For all three categories, higher numbers mean more of each alteration morphology.*

584 *Metamorphic rims are classed according to the percentage of each spot that included a metamorphic rim, from 0-100% rim.*

585 *Fractures were ranked on a qualitative scale from 0-3 where 3 represented a highly fractured spot location.*

586 *Mottled/Recrystallized was ranked similarly to metamorphic rim, on a scale from 0-100% according to the percentage of mottled*  
587 *or recrystallized domain in the spot location images.*

Class	Metamorphic Rims (0-100)		Fractures (0-3)		Mottled/Recrystallized (0-100)	
	Number	%	Number	%	Number	%
0/0	222	54.5	15	3.7	258	63.4
25/1	37	9.1	69	17.0	8	2.0
50/2	29	7.1	123	30.2	16	3.9
75/3	48	11.8	166	40.8	8	2.0
100	37	9.1	-	-	83	20.4
NA	34	8.4	34	8.4	34	8.4

588

589

590 As shown in Figure 8 (purple line), running the discordance dating procedure on the 222 analyses  
591 that do not contain any metamorphic rim growth within their visible area produces very similar  
592 results to the discordance dating procedure run on the entire 407 analysis dataset. This suggests  
593 that discordance dating is possible on samples that have only internal alteration and  
594 recrystallization, and new, metamorphic zircon rim growth is not required to obtain accurate  
595 discordance dating ages. This is in contrast to data obtained on mixed xenocryst-new rim zircon  
596 analyses that can be used to determine difficult-to-obtain ages from thin igneous rim growth zones  
597 (Rasmussen et al., 2023).

598

#### 599 4. Outlook and Future Directions:

600 Here we have showed that discordance dating may be used to date discordance-inducing events  
601 that affected detrital zircon populations. We have shown that this method provides several million-  
602 year age resolution on alteration events in rocks that experienced ~23 Ma fluid flow and  
603 metamorphism at temperatures that reached ~450°C. The high temperatures of metamorphism  
604 within the Tintic formation sample may lead to the perception that discordance dating is a tool that



605 is applicable to high-T metamorphic settings only. However, several pieces of data suggest that  
606 discordance dating may be an impactful method with wider applicability.

607

608 First, most zircon geochronologists pursue readily interpretable and therefore concordant data.  
609 Geochronologists tend to select spots targeting regions of high zircon quality and pick laser or ion  
610 probe analytical locations that are likely to retain a closed U-Pb system – a single metamorphic  
611 growth rim or a single domain of clearly igneous zircon. Additionally, what little discordant data  
612 may have been collected in laboratories around the world is commonly filtered based on a  
613 discordance threshold. Thus, there is no clear way to determine the general prevalence of  
614 discordant data in detrital zircon datasets. Additional analytical focus on discordant grain volumes  
615 may lead to additional insight into the value of discordant data for geochronological purposes.

616

617 Second, discordance dating will theoretically become more precise if discordant grains have older  
618 initial crystallization ages and the resetting event is relatively young. Due to the geometry of U-  
619 Pb isotope space, older grains experiencing more recent discordance-inducing geological events  
620 will provide a more precise estimate of lower intercept ages. However, though the Tintic formation  
621 contains grains with primary ages up to ~1.8 Ga, other more ancient grains would provide  
622 additional precision to any discordance dating analysis. The larger the age dispersion in detrital  
623 zircon crystallization ages, the more precision discordance dating would yield for Phanerozoic  
624 alteration events. Thus, a sediment that experienced less aggressive fluid flow or metamorphism,  
625 but that had older detrital zircon grains, may yield important lower intercept age information, with  
626 uncertainties on the order of a few million years.

627

628 Third, there is a growing body of evidence that discordance in zircon can be induced in a wide  
629 variety of low-temperature environments. Both experimental (Geisler et al., 2001; Pidgeon et al.,  
630 1966) and empirical (Geisler et al., 2002; Morris et al., 2015; Pidgeon et al., 2016; Zi et al., 2022)  
631 studies have documented large degrees, and sometimes near total, discordance at much lower  
632 temperatures (100–200 C) than the Tintic formation zircons analyzed in this work experienced.  
633 Thus, it is possible that many suites of detrital zircons experienced low-T hydrothermal fluid flow  
634 events that induced Pb-loss and/or recrystallization to such a degree that discordance dating could  
635 provide useful age information. This is particularly relevant as there are a limited number of  
636 geochronometers that are currently available to date reactive fluid flow events (brine migration,  
637 mineralizing fluid flow, low-T metamorphism, etc.) in sedimentary rocks– even imprecise age  
638 information is useful in such scenarios.

639

## 640 **5. Conclusions:**

641 We have documented a potential new tool for geochronologists to use to date in situ detrital zircon  
642 Pb loss events. We have shown the utility of this technique using extensive testing using synthetic  
643 datasets and ground-truthing by analyzing zircons within the well-studied Alta Stock metamorphic  
644 aureole. The discordance dating technique returns discordance ages of ~23 Ma, which is the  
645 expected age of fluid flow in this region. Our method may have significant applications to  
646 determining rates and absolute dates of diverse geologic phenomena; basin brine migration,  
647 mineralizing fluid flow, and low-grade burial metamorphism are just a few of the processes that  
648 may induce discordance in zircon analytical volumes such that it is amenable to discordance  
649 dating. Our preliminary data suggest that detailed in situ characterization and isotopic tools will  
650 help address fundamental questions on the nature of zircon U-Pb disturbance.



654 **Acknowledgements:**

655 This work was supported by Rudy L. Slingerland Early Career Professor of Geoscience funds  
656 awarded to JRR.

657

658 **Data Availability:**

659 The data reduction code and raw data used for discordance modeling is available here:

660 <https://github.com/jreimink-isotope-geochem/discordance-dating> and at the following Zenodo

661 DOI [10.5281/zenodo.13972610](https://doi.org/10.5281/zenodo.13972610)

662 and a public-facing easy-to-use Shiny app is available here:

663 [https://discordance.geosc.psu.edu/discordance\\_app/](https://discordance.geosc.psu.edu/discordance_app/)

664

665 **Competing Interests:**

666 The authors declare that they have no conflict of interest.

667

668 **Author Contributions:**

669 JRR, JD, and MKL conceived the study. AJS carried out sample collection. RB, ES, AC, and JG

670 separated zircons, collected U-Pb-TE data, and produced final results. JRR and JD carried out

671 modeling and sensitivity testing. All authors contributed to final data interpretation and manuscript

672 production.

673

674

675



676 **References:**

- 677 Andersen, T.: Correction of common lead in U–Pb analyses that do not report  $^{204}\text{Pb}$ , *Chemical*  
678 *Geology*, 192, 59–79, [https://doi.org/10.1016/S0009-2541\(02\)00195-x](https://doi.org/10.1016/S0009-2541(02)00195-x), 2002.
- 679 Andersen, T. and Elburg, M. A.: Open-system behaviour of detrital zircon during weathering: an  
680 example from the Palaeoproterozoic Pretoria Group, South Africa, *Geological Magazine*, 159,  
681 561–576, <https://doi.org/10.1017/S001675682100114X>, 2022.
- 682 Andersen, T., Elburg, M. A., and Magwaza, B. N.: Sources of bias in detrital zircon  
683 geochronology: Discordance, concealed lead loss and common lead correction, *Earth-Science*  
684 *Reviews*, 197, 102899, <https://doi.org/10.1016/j.earscirev.2019.102899>, 2019.
- 685 Anderson, A. J., Hanchar, J. M., Hodges, K. V., and van Soest, M. C.: Mapping radiation damage  
686 zoning in zircon using Raman spectroscopy: Implications for zircon chronology, *Chemical*  
687 *Geology*, 538, 119494, <https://doi.org/10.1016/j.chemgeo.2020.119494>, 2020.
- 688 Brenner, D. C., Passey, B. H., Holder, R. M., and Viete, D. R.: Clumped-Isotope Geothermometry  
689 and Carbonate U–Pb Geochronology of the Alta Stock Metamorphic Aureole, Utah, USA:  
690 Insights on the Kinetics of Metamorphism in Carbonates, *Geochemistry, Geophysics,*  
691 *Geosystems*, 22, e2020GC009238, <https://doi.org/10.1029/2020GC009238>, 2021.
- 692 Bromfield, C. S., Erickson, A. J., Haddadin, M. A., and Mehnert, H. H.: Potassium-argon ages of  
693 intrusion, extrusion, and associated ore deposits, Park City mining district, Utah, *Economic*  
694 *Geology*, 72, 837–848, <https://doi.org/10.2113/gsecongeo.72.5.837>, 1977.
- 695 Carter, A. and Bristow, C. S.: Detrital zircon geochronology: enhancing the quality of sedimentary  
696 source information through improved methodology and combined U–Pb and fission-track ...,  
697 *Basin Research*, 12, 47–57, <https://doi.org/10.1046/j.1365-2117.2000.00112.x>, 2000.
- 698 Cipar, J. H., Garber, J. M., Kylander-Clark, A. R. C., and Smye, A. J.: Active crustal differentiation  
699 beneath the Rio Grande Rift, *Nat. Geosci.*, 13, 758–763, [https://doi.org/10.1038/s41561-020-](https://doi.org/10.1038/s41561-020-0640-z)  
700 0640-z, 2020.
- 701 Clemens-Knott, D. and Gevedon, M.: Using discordant U–Pb zircon data to re-evaluate the El  
702 Paso terrane: Late Paleozoic tectonomagmatic evolution of east-central California (USA) and  
703 intense hydrothermal activity in the Jurassic Sierra Nevada arc, *Geosphere*, 19, 531–557,  
704 <https://doi.org/10.1130/GES02547.1>, 2023.
- 705 Cook, S. J., Bowman, J. R., and Forster, C. B.: Contact metamorphism surrounding the Alta Stock;  
706 finite element model simulation of heat- and  $^{18}\text{O}/^{16}\text{O}$  mass-transport during prograde  
707 metamorphism, *American Journal of Science*, 297, 1–55, <https://doi.org/10.2475/ajs.297.1.1>,  
708 1997.
- 709 Corfu, F.: Atlas of Zircon Textures, *Reviews in mineralogy and geochemistry*, 53, 469–500,  
710 <https://doi.org/10.2113/0530469>, 2003.



- 711 Crittenden, M., Stuckless, J., Kistler, R., and Stern, T.: Radiometric dating of intrusive rocks in the  
712 Cottonwood area, Utah | U.S. Geological Survey, *Journal of Research of the US Geological*  
713 *Survey*, 1, 173–178, 1973.
- 714 Davis, D. W.: Optimum linear regression and error estimation applied to U-Pb data, *Canadian*  
715 *Journal of Earth Sciences*, 19, 2141–2149, <https://doi.org/10.1139/e82-188>, 1982.
- 716 Davis, G. L., Hart, S. R., and Tilton, G. R.: Some effects of contact metamorphism on zircon ages,  
717 *Earth and Planetary Science Letters*, 5, 27–34, [https://doi.org/10.1016/S0012-821X\(68\)80006-8](https://doi.org/10.1016/S0012-821X(68)80006-8),  
718 1968.
- 719 Fedo, C. M., Sircombe, K. N., and Rainbird, R. H.: Detrital Zircon Analysis of the Sedimentary  
720 Record, *Reviews in mineralogy and geochemistry*, 53, 277–303,  
721 <https://doi.org/10.2113/0530277>, 2003.
- 722 Froude, D. O., Ireland, T. R., Ireland, T., Ireland, T. R., Kinny, P. D., Williams, I. S., Compston, W.,  
723 Williams, I. R., and Myers, J. S.: Ion microprobe identification of 4,100–4,200 Myr-old terrestrial  
724 zircons, *Nature*, 304, 616–618, <https://doi.org/10.1038/304616a0>, 1983.
- 725 Garber, J. M., Smye, A. J., Feineman, M. D., Kylander-Clark, A. R. C., and Matthews, S.:  
726 Decoupling of zircon U–Pb and trace-element systematics driven by U diffusion in eclogite-facies  
727 zircon (Monviso meta-ophiolite, W. Alps), *Contrib Mineral Petrol*, 175, 55,  
728 <https://doi.org/10.1007/s00410-020-01692-2>, 2020.
- 729 Gehrels, G.: Detrital Zircon U-Pb Geochronology: Current Methods and New Opportunities, in:  
730 *Tectonics of Sedimentary Basins*, John Wiley & Sons, Ltd, 45–62,  
731 <https://doi.org/10.1002/9781444347166.ch2>, 2011.
- 732 Gehrels, G.: Detrital Zircon U-Pb Geochronology Applied to Tectonics, *Earth and Planetary*  
733 *Sciences*, 42, 127–149, <https://doi.org/10.1146/annurev-earth-050212-124012>, 2014.
- 734 Geisler, T., Ulonska, M., Schleicher, H., Pidgeon, R. T., and van Bronswijk, W.: Leaching and  
735 differential recrystallization of metamict zircon under experimental hydrothermal conditions,  
736 *Contrib Mineral Petrol*, 141, 53–65, <https://doi.org/10.1007/s004100000202>, 2001.
- 737 Geisler, T., Pidgeon, R. T., Bronswijk, W. van, and Kurtz, R.: Transport of uranium, thorium, and  
738 lead in metamict zircon under low-temperature hydrothermal conditions, *Chemical Geology*,  
739 191, 141–154, [https://doi.org/10.1016/S0009-2541\(02\)00153-5](https://doi.org/10.1016/S0009-2541(02)00153-5), 2002.
- 740 Geisler, T., Schaltegger, U., and Tomaschek, F.: Re-equilibration of Zircon in Aqueous Fluids and  
741 Melts, *Elements*, 3, 43–50, <https://doi.org/10.2113/gselements.3.1.43>, 2007.
- 742 Grauert, B., Seitz, M. G., and Soptrajanova, G.: Uranium and lead gain of detrital zircon studied  
743 by isotopic analyses and fission-track mapping, *Earth and Planetary Science Letters*, 21, 389–  
744 399, [https://doi.org/10.1016/0012-821X\(74\)90178-2](https://doi.org/10.1016/0012-821X(74)90178-2), 1974.



- 745 Hiess, J., Condon, D. J., McLean, N., and Noble, S. R.: 238U/ 235U systematics in terrestrial  
746 uranium-bearing minerals, *Science*, 335, 1610–1614, 2012.
- 747 Hoskin, P. W. O.: The Composition of Zircon and Igneous and Metamorphic Petrogenesis,  
748 *Reviews in mineralogy and geochemistry*, 53, 27–62, <https://doi.org/10.2113/0530027>, 2003.
- 749 Hoskin, P. W. O. and Black, L. P.: Metamorphic zircon formation by solid-state recrystallization of  
750 protolith igneous zircon, *Journal of Metamorphic Geology*, 18, 423–439,  
751 <https://doi.org/10.1046/j.1525-1314.2000.00266.x>, 2002.
- 752 Kowallis, B. J., Ferguson, J., and Jorgensen, G. J.: Uplift along the salt lake segment of the  
753 Wasatch fault from apatite and zircon fission track dating in the little Cottonwood stock,  
754 *International Journal of Radiation Applications and Instrumentation. Part D. Nuclear Tracks and*  
755 *Radiation Measurements*, 17, 325–329, [https://doi.org/10.1016/1359-0189\(90\)90054-2](https://doi.org/10.1016/1359-0189(90)90054-2), 1990.
- 756 Kusiak, M. A., Dunkley, D. J., Wirth, R., Whitehouse, M. J., Wilde, S. A., and Marquardt, K.:  
757 Metallic lead nanospheres discovered in ancient zircons, *Proceedings of the National Academy*  
758 *of Sciences*, 112, 201415264, <https://doi.org/10.1073/pnas.1415264112>, 2015.
- 759 Kusiak, M. A., Wirth, R., Wilde, S. A., and Pidgeon, R. T.: Metallic lead (Pb) nanospheres  
760 discovered in Hadean and Eoarchean zircon crystals at Jack Hills, *Sci Rep*, 13, 895,  
761 <https://doi.org/10.1038/s41598-023-27843-6>, 2023.
- 762 Landing, E., Schmitz, M. D., Geyer, G., Trayler, R. B., and Bowring, S. A.: Precise early Cambrian  
763 U–Pb zircon dates bracket the oldest trilobites and archaeocyaths in Moroccan West Gondwana,  
764 *Geological Magazine*, 158, 219–238, <https://doi.org/10.1017/S0016756820000369>, 2021.
- 765 Matthews, W., Guest, B., and Madronich, L.: Latest Neoproterozoic to Cambrian detrital zircon  
766 facies of western Laurentia, *Geosphere*, 14, 243–264, <https://doi.org/10.1130/GES01544.1>,  
767 2017.
- 768 Mattinson, J. M.: Zircon U–Pb chemical abrasion (“CA-TIMS”) method: Combined annealing and  
769 multi-step partial dissolution analysis for improved precision and accuracy of zircon ages,  
770 *Chemical Geology*, 220, 47–66, <https://doi.org/10.1016/j.chemgeo.2005.03.011>, 2005.
- 771 Mattinson, J. M.: Revolution and Evolution: 100 Years of U–Pb Geochronology, *Elements*, 9, 53  
772 57, <https://doi.org/10.2113/gselements.9.1.53>, 2013.
- 773 Mezger, K. and Krogstad, E. J.: Interpretation of discordant U–Pb zircon ages: An evaluation,  
774 *Journal of Metamorphic Geology*, 15, 127–140, <https://doi.org/10.1111/j.1525-1314.1997.00008.x>, 1997.
- 776 Moore, J. N. and Kerrick, D. M.: Equilibria in siliceous dolomites of the Alta aureole, Utah,  
777 *American Journal of Science*, 276, 502–524, <https://doi.org/10.2475/ajs.276.4.502>, 1976.



- 778 Morris, G. A., Kirkland, C. L., and Pease, V.: Orogenic paleofluid flow recorded by discordant  
779 detrital zircons in the Caledonian foreland basin of northern Greenland, *Lithosphere*, 7, 138  
780 143, <https://doi.org/10.1130/l420.1>, 2015.
- 781 Moser, D. E., Davis, W. J., Reddy, S. M., Flemming, R. L., and Hart, R. J.: Zircon U–Pb strain  
782 chronometry reveals deep impact-triggered flow, *Earth and Planetary Science Letters*, 277, 73–  
783 79, <https://doi.org/10.1016/j.epsl.2008.09.036>, 2009.
- 784 Moser, D. E., Cupelli, C. L., Barker, I. R., Flowers, R. M., Bowman, J. R., Wooden, J., and Hart, J. R.:  
785 New zircon shock phenomena and their use for dating and reconstruction of large impact  
786 structures revealed by electron nanobeam (EBSD, CL, EDS) and isotopic U–Pb and (U–Th)/He  
787 analysis of the Vredefort dome This article is one of a series of papers published in this Special  
788 Issue on the theme of Geochronology in honour of Tom Krogh., *Canadian Journal of Earth  
789 Sciences*, 48, 117–139, <https://doi.org/10.1139/e11-011>, 2011.
- 790 Nasdala, L., Pidgeon, R. T., Wolf, D., and Irmer, G.: Metamictization and U–Pb isotopic  
791 discordance in single zircons: a combined Raman microprobe and SHRIMP ion probe study,  
792 *Mineralogy and Petrology*, 62, 1–27, <https://doi.org/10.1007/BF01173760>, 1998.
- 793 Nasdala, L., Hanchar, J. M., Rhede, D., Kennedy, A. K., and Váczi, T.: Retention of uranium in  
794 complexly altered zircon: An example from Bancroft, Ontario, *Chemical Geology*, 269, 290–300,  
795 <https://doi.org/10.1016/j.chemgeo.2009.10.004>, 2010.
- 796 Olierook, H. K. H., Kirkland, C. L., Barham, M., Daggitt, M. L., Hollis, J., and Hartnady, M.:  
797 Extracting meaningful U–Pb ages from core–rim mixtures, *Gondwana Research*, 92, 102–112,  
798 <https://doi.org/10.1016/j.gr.2020.12.021>, 2021.
- 799 Pidgeon, R. T., O’Neil, J. R., and Silver, L. T.: Uranium and Lead Isotopic Stability in a Metamict  
800 Zircon under Experimental Hydrothermal Conditions, *Science*, 154, 1538–1540,  
801 <https://doi.org/10.1126/science.154.3756.1538>, 1966.
- 802 Pidgeon, R. T., Nemchin, A. A., and Whitehouse, M. J.: The effect of weathering on U–Th–Pb and  
803 oxygen isotope systems of ancient zircons from the Jack Hills, Western Australia, *Geochimica et  
804 Cosmochimica Acta*, 197, 1–62, <https://doi.org/10.1016/j.gca.2016.10.005>, 2016.
- 805 Powerman, V. I., Buyantuev, M. D., and Ivanov, A. V.: A review of detrital zircon data treatment,  
806 and launch of a new tool ‘Dezirteer’ along with the suggested universal workflow, *Chemical  
807 Geology*, 583, 120437, <https://doi.org/10.1016/j.chemgeo.2021.120437>, 2021.
- 808 Rasmussen, K. L., Falck, H., Elongó, V., Reimink, J., Luo, Y., Pearson, D. G., Ootes, L., Creaser, R. A.,  
809 and Lecumberri-Sanchez, P.: The source of tungsten-associated magmas in the northern  
810 Canadian Cordillera and implications for the basement, *Geology*, 51, 657–662,  
811 <https://doi.org/10.1130/G51042.1>, 2023.



- 812 Reddy, S. M., Timms, N. E., Trimby, P., Kinny, P. D., Buchan, C., and Blake, K.: Crystal-plastic  
813 deformation of zircon: A defect in the assumption of chemical robustness, *Geology*, 34, 257–4,  
814 <https://doi.org/10.1130/g22110.1>, 2006.
- 815 Reimink, J. R., Davies, J. H. F. L., Waldron, J. W. F., and Rojas, X.: Dealing with discordance: a  
816 novel approach for analysing U–Pb detrital zircon datasets, *Journal of the Geological Society*,  
817 173, 2015–114 585, <https://doi.org/10.1144/jgs2015-114>, 2016.
- 818 Resentini, A., Andò, S., Garzanti, E., Malusà, M. G., Pastore, G., Vermeesch, P., Chanvry, E., and  
819 Dall’Asta, M.: Zircon as a provenance tracer: Coupling Raman spectroscopy and UPb  
820 geochronology in source-to-sink studies, *Chemical Geology*, 555, 119828,  
821 <https://doi.org/10.1016/j.chemgeo.2020.119828>, 2020.
- 822 Salje, E. K. H., Chrosch, J., and Ewing, R. C.: Is “metamictization” of zircon a phase transition?,  
823 *American Mineralogist*, 84, 1107–1116, <https://doi.org/10.2138/am-1999-7-813>, 1999.
- 824 Schaltegger, U., Schmitt, A. K., and Horstwood, M. S. A.: U–Th–Pb zircon geochronology by ID-  
825 TIMS, SIMS, and laser ablation ICP-MS: recipes, interpretations, and opportunities, *Chemical*  
826 *Geology*, 402, 1–70, <https://doi.org/10.1016/j.chemgeo.2015.02.028>, 2015.
- 827 Schoene, B.: *U–Th–Pb Geochronology*, Elsevier, 2014.
- 828 Schoonover, E., Garber, J. M., Smye, A. J., Kylander-Clark, A., and Reimink, J. R.: Snapshots of  
829 magmatic evolution revealed by zircon depth profiling, *Earth and Planetary Science Letters*, 647,  
830 2024.
- 831 Seydoux-Guillaume, A.-M., Bingen, B., Paquette, J.-L., and Bosse, V.: Nanoscale evidence for  
832 uranium mobility in zircon and the discordance of U–Pb chronometers, *Earth and Planetary*  
833 *Science Letters*, 409, 43–48, <https://doi.org/10.1016/j.epsl.2014.10.044>, 2015.
- 834 Stacey, J. S. and Kramers, J. D.: Approximation of terrestrial lead isotope evolution by a two-  
835 stage model, *Earth and planetary science letters*, 26, 207–221, [https://doi.org/10.1016/0012-](https://doi.org/10.1016/0012-821x(75)90088-6)  
836 [821x\(75\)90088-6](https://doi.org/10.1016/0012-821x(75)90088-6), 1975.
- 837 Stearns, M. A., Bartley, J. M., Bowman, J. R., Forster, C. W., Beno, C. J., Riddle, D. D., Callis, S. J.,  
838 and Udy, N. D.: Simultaneous Magmatic and Hydrothermal Regimes in Alta–Little Cottonwood  
839 Stocks, Utah, USA, Recorded Using Multiphase U–Pb Petrochronology, *Geosciences*, 10, 129,  
840 <https://doi.org/10.3390/geosciences10040129>, 2020.
- 841 Trachenko, K., Dove, M. T., and Salje, E. K. H.: Large swelling and percolation in irradiated zircon,  
842 *J. Phys.: Condens. Matter*, 15, L1, <https://doi.org/10.1088/0953-8984/15/2/101>, 2002.
- 843 Vermeesch, P.: On the visualisation of detrital age distributions, *Chemical Geology*, 312–313,  
844 190–194, <https://doi.org/10.1016/j.chemgeo.2012.04.021>, 2012.



- 845 Vermeesch, P.: IsoplotR: A free and open toolbox for geochronology, *Geoscience Frontiers*, 9,  
846 1479–1493, <https://doi.org/10.1016/j.gsf.2018.04.001>, 2018.
- 847 Vermeesch, P.: On the treatment of discordant detrital zircon U–Pb data, *Geochronology*, 3,  
848 247–257, <https://doi.org/10.5194/gchron-3-247-2021>, 2021.
- 849 York, D.: Least squares fitting of a straight line with correlated errors, *Earth and planetary*  
850 *science letters*, 5, 320–324, [https://doi.org/10.1016/s0012-821x\(68\)80059-7](https://doi.org/10.1016/s0012-821x(68)80059-7), 1968.
- 851 Zhang, M., Salje, E. K. H., Farnan, I., Graeme-Barber, A., Daniel, P., Ewing, R. C., Clark, A. M., and  
852 Leroux, H.: Metamictization of zircon: Raman spectroscopic study, *J. Phys.: Condens. Matter*, 12,  
853 1915, <https://doi.org/10.1088/0953-8984/12/8/333>, 2000.
- 854 Zi, J.-W., Rasmussen, B., Muhling, J. R., and Fletcher, I. R.: In situ U-Pb and geochemical evidence  
855 for ancient Pb-loss during hydrothermal alteration producing apparent young concordant zircon  
856 dates in older tuffs, *Geochimica et Cosmochimica Acta*, 320, 324–338,  
857 <https://doi.org/10.1016/j.gca.2021.11.038>, 2022.

858